Structure-function coupling and decoupling during movie-watching and resting-state: Novel insights bridging EEG and structural imaging

Venkatesh Subramani[1,2], Giulia Lioi[1], Karim Jerbi[2,3,4], and Nicolas Farrugia*[1]

[1]IMT Atlantique, Lab-STICC UMR CNRS 6285 F-29238, France

[2]Cognitive and Computational Neuroscience Laboratory (CoCo Lab), Psychology Department, Université de Montréal, Québec, Canada

[3]Mila (Québec AI research Institute), Montréal, QC, Canada

[4]UNIQUE Center (Québec Neuro-AI research Center), QC, Canada

April 5, 2024

Keywords: structure-function coupling, EEG, structural connectivity, graph signal processing, movie watching, resting-state

Abstract: The intricate structural and functional architecture of the brain enables a wide range of cognitive processes ranging from perception and action to higher-order abstract thinking. Despite important progress, the relationship between the brain's structural and functional properties is not yet fully established. In particular, the way the brain's anatomy shapes its electrophysiological dynamics remains elusive. The electroencephalography (EEG) activity recorded during naturalistic tasks is thought to exhibit patterns of coupling with the underlying brain structure that vary as a function of behavior. Yet these patterns have not yet been sufficiently quantified. We address this gap by jointly examining individual Diffusion-Weighted Imaging (DWI) scans and continuous EEG recorded during video-watching and

*Correspondence: nicolas.farrugia@imt-atlantique.fr

resting state, using a Graph Signal Processing (GSP) framework. By decomposing the structural graph into Eigenmodes and expressing the EEG activity as an extension of anatomy, GSP provides a way to quantify the structure-function coupling. Our findings indicate that the EEG activity in the sensorimotor cortex is strongly coupled with brain structure, while the activity in higher-order systems is less constrained by anatomy, i.e., shows more flexibility. In addition, we found that watching videos was associated with stronger structure-function coupling in the sensorimotor cortex, as compared to resting-state data. Together, this unprecedented characterization of the link between structure and function using continuous EEG during naturalistic behavior underscores the role of anatomy in shaping ongoing cognitive processes. Taken together, by combining the temporal and spectral resolution of EEG and the methodological advantages of GSP, our work sheds new light onto the anatomo-functional organization of the brain.

1 Introduction

The functioning of various natural systems is fundamentally constrained by their structure. Analogous to the way the pitch and timbre of music emanating from a flute are intricately tied to the precise design and arrangement of its cylindrical tube, holes, and keys, the functionality of the brain is constrained by its anatomical scaffold (Hagmann et al., 2008; Lynn & Bassett, 2019). However, despite important progress, the precise extent of the association between the brain's anatomical hardwiring and its dynamic functional properties is not yet fully understood. Indeed, characterizing the structure-function relationship in neural processes is currently at the forefront of the neuroimaging community's interest, as illustrated for instance by a recent seminal publication (Pang et al., 2023a) and the various commentary papers it has sparked (Faskowitz et al., 2023; Pang et al., 2023b; Patil et al., 2023).

One line of inquiry that has proven to be promising in investigating structure-function interplay is via spectral graph theory (Spielman, 2007) which provides a framework to express connectivity matrix in graph spectral components using eigenvectors (or eigenmodes) decomposition. In the context of studying the brain, eigenmodes are derived from the Laplacian of connectivity graphs (Bajada et al., 2020), i.e., structural connectome (anatomical links) or functional connectome (statistical dependence between pairs of brain regions). While spectral graph theory analyzes connectivity graphs, an elegant framework that allows to jointly analyze a brain signal onto a connectivity graph is Graph Signal processing (GSP) (Shuman et al., 2013). In GSP, Laplacian eigenvectors are used to decompose the signal in graph Fourier modes by defining a Graph Fourier Transform, thus translating Fourier analysis (and a series of operations such as

convolution and filtering) on graphs. GSP is a powerful tool to specifically investigate structure-function interplay and has been successfully applied to analyze brain data in several recent studies (Glomb et al., 2020; Medaglia et al., 2015; Preti & Van De Ville, 2019). The connectivity/GSP framework can be seen as complementary to the classical approach of mapping brain functions in discrete cortical parcellations as it allows for a decomposition of brain activity or structure as a continuum of spectral components (see Lioi et al., 2021 for a perspective review). Crucially, increasing evidence of the functional relevance of these spectral components (also named connectivity gradients or harmonics) has been shown using functional Magnetic Resonance Imaging (fMRI) (Atasoy et al., 2016; Glomb et al., 2021; Margulies et al., 2016), Electroencephalography (EEG) (Glomb et al., 2020), Magneto-encephalography (MEG) (Griffa & Preti, 2022) and microstructural brain data (Paquola et al., 2019).

Pioneering studies with resting-state fMRI data have investigated macroscale brain organization and found that the first connectivity gradient reveals a hierarchy spanning between unimodal (sensory systems) to transmodal (higher-order systems) association regions (Margulies et al., 2016). To study how the structure-function coupling is organized in the brain, Preti and Van de Ville (Preti & Van De Ville, 2019) developed a metric from GSP called the Structural-Decoupling Index (SDI). The term *Coupling* in this context refers to brain activity that closely matches the underlying structure, whereas the *decoupling* refers to brain activity less tied to the structure. In their study, they investigated the dependency of fMRI signal on the underlying structural connectome estimated with Diffusion-Weighted Imaging (DWI) during rest and found a similar hierarchy revealed by Margulies et al., 2016, with the coupling of fMRI activity gradually decreasing along the unimodal-transmodal axis (Preti & Van De Ville, 2019). While the majority of the contributions in this line of work has used MRI imaging, a handful of studies have attempted to characterize the dependency of the electrophysiological signals on the structural connectome. For instance, SDI has been used to quantify the relationship of fast temporal activity with MEG in Griffa and Preti, 2022, indicating a different gradient of organization as compared with fMRI, with coupled sensory areas (task-positive) and decoupled default mode network areas (task negative). Other recent studies investigating EEG visual and auditory event-related potentials found that during these tasks, the cortical activity can be compactly represented by a sparse set of structural connectome harmonics (Glomb et al., 2020; Rué-Queralt et al., 2021, 2023). Structure-Function coupling of the EEG has also been studied during epileptic seizures (Rigoni et al., 2023) with results showing that epileptic activity is more coupled to a generic structural graph during the spike. These studies focused on characterising the interplay between anatomical structure and EEG activity in well isolated and/or evoked events. This is in contrast with the works applying the GSP framework to fMRI which have primarily focused on resting state. Moreover, to the best of our knowledge, all the brain studies using the gradients/GSP framework have considered a common structural graph, estimated from either unrelated healthy subjects (such as

in Griffa and Preti, 2022; Preti and Van De Ville, 2019) or as the average connectivity matrix across the population (Rué-Queralt et al., 2023). Taken together, despite the important progress in probing the nature of structure-function coupling through the lens of task-based electrophysiological responses, the relationship between the continuous EEG and the underlying structural connectivity remains elusive.

This study tackles for the first time the fundamental question of the relationship between continuous EEG activity and individual structural connectomes using GSP. We estimate EEG cortical activity during rest and video watching and use the Laplacian eigenmodes of the individual structural graph to decompose the source-localized activity into graph-informed components. We then estimate the SDI metric to characterize the structure-function coupling relationship of EEG in different frequency bands. Precisely, we address the following open questions: a) How is the continuous EEG during rest and video watching constrained by the underlying individual structural connectivity? b) Are the rest and video-watching EEG activities constrained by the structure in the same way? c) Does the structure-function coupling exhibit different patterns for different EEG frequency bands? d) Is the functional-structural relationship significantly modulated by salient events during video watching? Using high quality EEG and individual DWI data from a large open access dataset and rigorous validation/estimation of GSP derived metrics, we provide novel insights into how the anatomy shapes the continuous electrophysiological activity of the human brain, and how this relationship is modulated by behavior.

2 Methods

2.1 Data and Preprocessing

We analyzed a subset of the EEG and DWI data acquired by the Healthy Brain Network (HBN) (Langer et al., 2017). In particular, we used high-density EEG recorded using a 128-channel Geodesic Hydrocel system at a sampling frequency of 500 Hz while subjects were (i) resting with open eyes (100 sec), (ii) watching a clip from Despicable Me 2 (Video 1 [1], 170 sec) and (iii) watching a clip from Fun with Fractals (Video 2 [2], 162 sec). The released EEG data includes preprocessing steps such as electrode data quality checks, notch-filter at 60Hz, high-pass filter at 0.1Hz and artifact signal correction (more details in Langer et al., 2017). In addition, we excluded 27 electrodes and only selected subjects having a good EEG quality determined as part of the quality assessment in Nentwich et al., 2020. We identified a group of 43 subjects (aged 14 - 21.8) based on the following criteria: i) age of at least 14 years; ii)

[1] https://www.youtube.com/watch?v=HNXxJIhVALI
[2] https://www.youtube.com/watch?v=XwWyTts06tU

having both resting state and video watching EEG; iii) undergone DWI scans in order to estimate the subject-specific structural connectome.

2.2 EEG Source Reconstruction

We used Freesurfer (Fischl, 2012), Boundary Element Method (BEM), and exact Low-Resolution Electromagnetic Tomography (eLORETA) (Pascual-Marqui et al., 2011) to estimate the cortical sources. To define the cortical surface and cortical mesh, we used Freesurfer's fsaverage version 5. We characterized the electromagnetic properties of different brain segments using BEM and used the consensus montage of the 128-EEG channel array while computing the forward operator. We used subject-specific eyes-closed and eyes-open resting state (20 sec) to compute the noise-covariance matrix for estimating the cortical sources for resting-state eyes-open and video-watching EEG respectively. We computed the inverse solution using eLORETA (Pascual-Marqui et al., 2011), a minimum-norm estimate algorithm as implemented in MNE-Python (Gramfort et al., 2013). We estimated EEG cortical sources for the entire time series on the 20484 vertices of the cortical mesh, and then parcellated the full-length signal into 360 Regions of Interest (ROIs) of the HCP-MMP atlas (Glasser et al., 2016). We bandpassed the full-bandwidth EEG signal into the standard frequency bands: θ (4 - 8Hz), α (8 - 13Hz), Low β (13 - 20Hz), High β (20 - 30Hz), and γ (30 - 40Hz). To this end, we first downsampled the wideband signal to 125Hz (anti-aliasing filter; performed using `mne.epochs.resample()`), followed by applying a fifth-order butterworth filter (implemented in `scipy.signal.butter()`). We then applied the Hilbert Transform to extract the signal envelopes for the narrow-band signals (implemented in `scipy.signal.hilbert()`). We then assessed the structure-function relationship for two types of EEG signals: 1) EEG wideband signal; 2) the narrow-band cortical EEG envelopes in the different frequency bands across different conditions (Video 1, Rest, and Video 2).

2.3 Structural graph

2.3.1 Connectome reconstruction

We used Qsiprep (Cieslak et al., 2021) to process the structural (T1w) and DWI images in the Brain Imaging Data Structure (BIDS) format. The preprocessing pipeline included head motion correction, susceptibility distortion correction, MP-PCA denoising, coregistration to T1w images, spatial normalization using ANTs, and tissue segmentation (Cieslak et al., 2021). We used the MRtrix3 (Tournier et al., 2019) pipeline available through Qsiprep for fiber reconstruction. In particular, we employed multi-shell

multi-tissue constrained spherical deconvolution (`mrtrix_multishell_msmt_ACT-hsvs`) for estimating the fiber orientation distribution using the Dhollander algorithm (Dhollander et al., 2019). We then applied `tckgen`, specifically `iFOD2`, a probabilistic tracking method that generates 10^7 streamlines, with the weights for each streamline calculated using `SIFT2` (Smith et al., 2015). We set the T1w segmentation reconstructed through Freesurfer as an anatomical constraint. We used the same HCP-MMP atlas for fiber segmentation and we quantify the structural relationship between pairs of ROIs as the density of the fibers calculated as the sum of the fibers connecting two regions divided by the region volumes as in (Preti & Van De Ville, 2019). The estimated individual connectomes were then used to assess subject-specific structure-function coupling.

2.3.2 Eigendecomposition of the connectome

Structural connections between different brain regions can be effectively modeled as graphs (Bassett & Sporns, 2017; Lynn & Bassett, 2019) (Fig 1a), and the spectral properties of the graphs can be further studied using the Laplacian operator (Spielman, 2007). Let us consider an undirected weighted graph $G =< V, \mathcal{E}, W >$, where V is a set of N elements called vertices and $\mathcal{E} \subset V \times V$ the set of edges connecting unordered pairs of vertices with scalar weights w. In this work, the nodes correspond to HCP-MMP ROIs, and the edges represent white matter fibers links between those nodes weighted by the strength of the connections (e.g. fiber density). The degree matrix $\mathbf{D}$ of a graph G, is a diagonal matrix such that $D_{i,j} = \sum_{k=1}^{N} w_{ij}$ if $i = j$ and 0 otherwise. The Adjacency Matrix $\mathbf{A}$ is a square matrix of dimension $N \times N$ in which each element is different from zero only if the corresponding edge exists. Given $\mathbf{A}$ and $\mathbf{D}$ we can define a Laplacian operator. In line with previous studies such as Preti and Van De Ville, 2019, we used the symmetric normalized Laplacian, which is defined as $\mathbf{L} = \mathbf{I}$ - $\mathbf{D^{-1/2}}\ \mathbf{AD^{-1/2}}$, where $\mathbf{I}$ is identity matrix. $\mathbf{L}$ the Laplacian is a real symmetric matrix and thus can be diagonalized as

$$\mathbf{L} = \mathbf{U}\Lambda\mathbf{U}^{\top} \tag{1}$$

where $\mathbf{U}$ denotes the base of orthogonal eigenvectors and $\mathbf{\Lambda}$ the diagonal matrix of eigenvalues, sorted in increasing order. Eigenvectors (often referred to as eigenmodes) capture the spatial frequencies of the graph and are ordered by an increasing level of spatial frequency (i.e., low frequency to high frequency). In particular, low-frequency eigenmodes capture the main axes of information diffusion in the network while high-frequency eigenmodes are more scattered, as illustrated in Fig 1b.

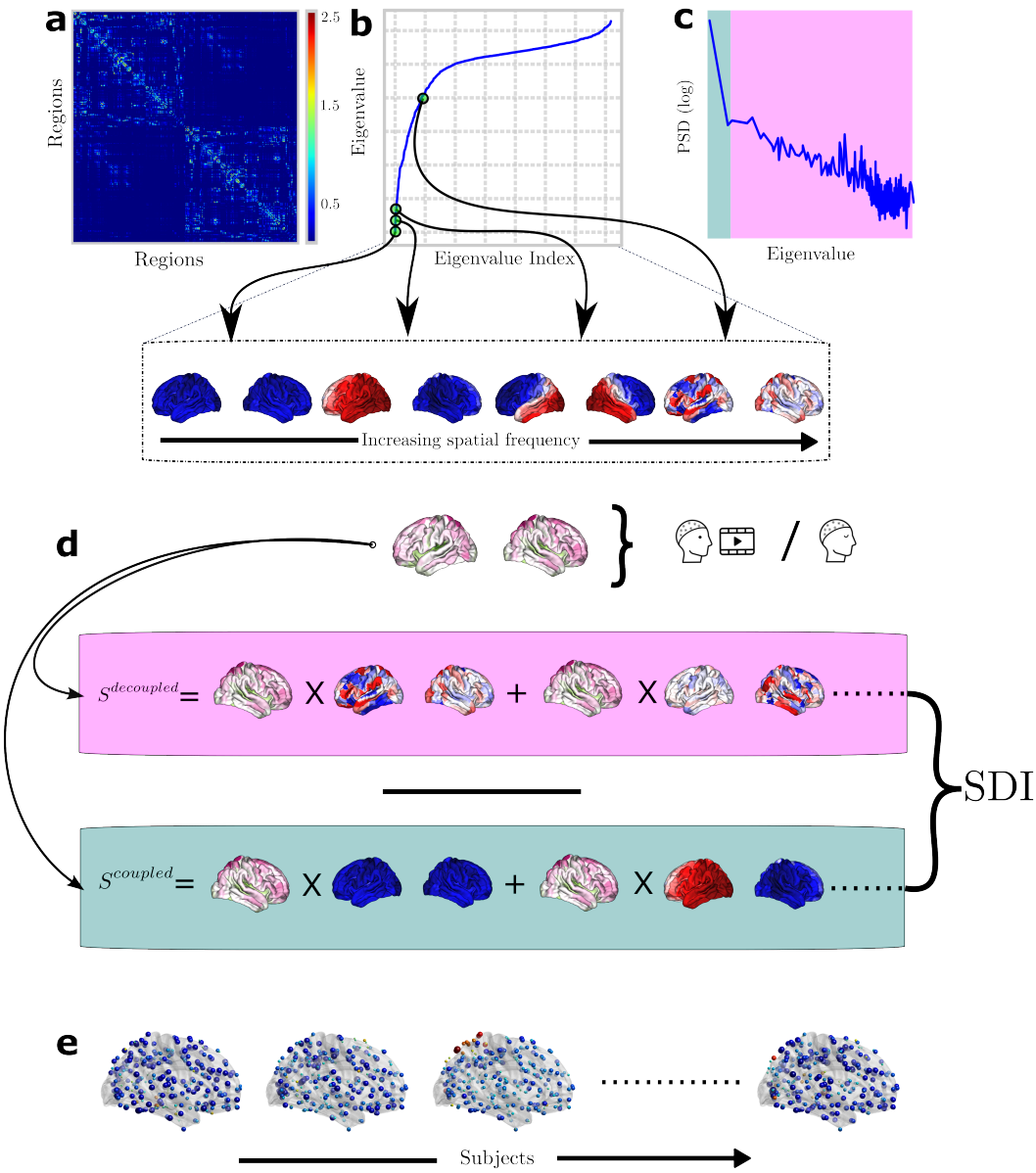

Figure 1: Illustration of the methods pipeline. **a** The structural connectome is estimated for each individual (here we show the consensus structural graph in natural logarithmic scale). **b** The spectral decomposition of the structural connectome Laplacian results in eigenmodes that capture the spatial harmonics progressing from the smoothest (first eigenmode, corresponding to the lower part of the spectrum) to high frequency eigenmodes, corresponding to higher part of the spectrum. Eigenvectors are orthogonal to each other, so the EEG activity can be expressed as a weighted linear combination of them using the Graph Fourier Transform. **c** Averaged Power Spectral Density (PSD) of EEG graph signals ($\ell 2$-normed) revealing the power distribution of the source EEG on the graph. Median power split criterion was used to split the graph power spectrum in order to identify the low/high-band pass filters cut-off frequency. **d** EEG cortical signals are high and low pass-filtered using graph filters to isolate the activity which is respectively decoupled and coupled to the underlying structural graph. The SDI index is calculated as the ratio between the decoupled and coupled activity (Preti & Van De Ville, 2019). **e** SDIs for a few representative subjects.

2.3.3 Graph Fourier Transform and Structural Decoupling Index estimation

The set of scalar values residing on the vertices of the graph is called graph signal. In this work the graph signal S_t is the cortical EEG at time t associated with each node (ROI) in the graph. Eigendecomposition provides a Fourier basis for the graph signal, enabling the application of classic signal processing techniques such as Fourier transform or filtering. The Graph Fourier Transform (GFT) transforms the signals defined on the vertices of a graph into the graph spectral domain

$$\hat{S}_t = \mathbf{U}^\top S_t \tag{2}$$

The original signal S_t at time t can be reconstructed back using Inverse GFT (equation 3).

$$S_t = \mathbf{U}\hat{S}_t \tag{3}$$

Once we have the notion of a graph Fourier transform, we can generalize from classic Fourier domain to define frequency filtering, or graph spectral filtering such as $S_t^{out} = \hat{h}(\mathbf{L})S_t^{in}$ where

$$\hat{h}(\mathbf{L}) = \mathbf{U}\begin{pmatrix} \hat{h}(\lambda_0) & \cdots & 0 \\ \vdots & \ddots & \vdots \\ 0 & \cdots & \hat{h}(\lambda_N) \end{pmatrix}\mathbf{U}^\top \tag{4}$$

We can therefore isolate the low frequency and high frequency components of the graph signal with a graph low-pass and high-pass ideal filters,

$$S_t^{coupled} = \hat{h}^{low}(\mathbf{L})S_t \tag{5}$$

$$S_t^{decoupled} = \hat{h}^{high}(\mathbf{L})S_t \tag{6}$$

where $\hat{h}^{low}(\mathbf{L})$ and $\hat{h}^{high}(\mathbf{L})$ act as band-pass filters, extracting the low- and high-frequency spatiotemporal activity denoted as $S_t^{coupled}$ and $S_t^{decoupled}$. Specifically, $\hat{h}^{low}(\mathbf{L})$ retains only the first C diagonal elements and pads the rest with zeros while $\hat{h}^{high}(\mathbf{L})$ keeps only the diagonal elements corresponding to the last $N - C$ eigenvalues. Notably, $S_t^{coupled}$ is the EEG activity that is closely aligned to the structural graph, while the high graph frequency activity $S_t^{decoupled}$ is less constrained by the underlying network (Lioi et al., 2021). The Structural-decoupling index (SDI) (Preti & Van De Ville, 2019) is defined as the ratio between the norm of $S_t^{decoupled}$ and $S_t^{coupled}$. We applied binary logarithm as in Preti

and Van De Ville, 2019, thus the positive and negative SDI values indicates decoupling and coupling, respectively. We computed SDIs for each region across all subjects and the resulting spatial maps are presented in Fig 1e for a few subjects. As in Preti and Van De Ville, 2019, we identified as cut-off frequency between low and high frequencies the one that splits the spectrum into two parts with equal energy (median-frequency)(Fig 1b and c). The cut-off frequency varies among subjects but its median is the same across conditions (Video 1, Rest and Video 2: median $C = 2$ for the wideband EEG).

2.4 Decoding of the SDI maps

To establish the functional relevance of SDI maps, we performed a NeuroSynth (Yarkoni et al., 2011) meta-analysis similar to previous studies (Margulies et al., 2016; Preti & Van De Ville, 2019). First, unthresholded SDI maps were segmented into bins with a 10%ile increment and binarized. Next, we used `ROIAssociationDecoder` function in NiMare to decode the 10 binary masks using the Neurosynth database. This database contains over 500,000 activation maps from over 14K studies (more details in NiMare website and in Salo et al., 2022). `ROIAssociationDecoder` synthesizes this entire database and perform spatial correlation between input masks and the meta-analytic maps to extract the relevant topic-terms. We then transformed the resulting correlation coefficient into z-statistics and showed significant results corresponding to a p-value$<$0.001. Note that unlike the previous studies that performed decoding (Margulies et al., 2016), for an easier comparison between task conditions and with the previous studies, we manually ordered the topics based on the hierarchy in lower order to higher order systems.

2.5 Null models and statistical analysis

Firstly, we assessed the level of statistical significance of SDI maps. To do this, we compared the empirical SDI with graph-informed surrogate SDI, following the methodology to obtain null models outlined in Preti and Van De Ville, 2019. In particular, to generate graph-informed surrogates, we employed spectral randomization of the graph (Pirondini et al., 2016) that randomizes the phase of the GFT coefficients, while preserving the auto-correlation of the graph Laplacian.

$$S_t^{surrogate} = \mathbf{U}^T \mathbf{P} \hat{S}_t \tag{7}$$

Here, $\mathbf{P}$ represents a diagonal matrix with random $+1$ and -1 enforcing randomization for the inverse GFT to produce the surrogate cortical signal. A total of 19 surrogates were generated, maintaining $\alpha = 1/(1 + 19) = 0.05$. We computed surrogate SDI for each condition (Video 1, Rest, and Video

2) using the surrogate EEG time series, in the same way as for the empirical SDI. The surrogate SDIs served as a noise floor against which individual empirical SDIs were tested. We then assessed consistency across subjects using a threshold determined based on binomial cumulative distribution with the following parameters: 43 subjects, 100 trials, the rate of success at p=0.05 (Preti & Van De Ville, 2019).

We also assessed differences between video-watching and rest with a paired statistical test between the empirical SDIs. Within each EEG frequency band, we performed a t-test between the conditions followed by FDR-correction ($\alpha = 0.05$).

Finally, we assessed the difference in structure-function coupling patterns across EEG frequency bands. To do this, we aggregated the SDIs from HCP-MMP ROIs into Yeo-Krienen networks (Yeo et al., 2011) and computed Spearman's ρ between pairs of frequency bands.

2.6 Test-retest reliability with Video 2

To test the robustness of the findings presented for Video 1, we performed the same analysis for Video 2. We used intra-class correlation coefficient (ICC) as the reliability index (Koo & Li, 2016). The ICC estimates and the 95% confidence intervals were computed using the Pingouin package in Python. Specifically, we used the two-way random-effects model of ICC to determine the inter-rater reliability between two videos, treating the Video 1 and 2 as independent raters. The choice of the random-effects model for ICC accommodates potential sources of variability that could influence EEG recordings, including different days, variations in equipment, and different experimenters.

3 Results

3.1 Brain-wide coupling and focal decoupling patterns across video and rest

We began by investigating the structure-function coupling of the wideband EEG signals during video-watching and the resting-state. First, we show in Fig 2a global brain activity patterns during Video and Rest, using averaged spatial map of the source-localized wideband EEG across subjects and time. Resulting spatial maps were then zscored to highlight the salient regions. These two maps summarize the brain activity over the entire period of video and rest, and show average brain-wide activation that is mostly similar between conditions. As our focus is investigating structure-function coupling, and due to the continuous nature of the signals, we did not seek to compare brain activity statistically.

Average graph PSD for the video-watching and resting state cortical signal are presented in Fig 2b for video (in magenta) and rest (in olive). To calculate the average graph PSD across subjects we considered the consensus graph. The graph PSD of the cortical activity has a 1/f-like shape, with the largest part of the power in the low frequencies. This indicates that the low-frequency connectome harmonics carry dominant role in explaining the given cortical signal.

For the rest of the results, we quantified the structure-function relationship using individual connectomes. The group-level SDI map during video-watching is represented in Fig 2c. This map, thresholded using group-level significance (see section 2.5) highlights the coupling (blue) and decoupling (red) of the electrophysiology on the anatomical scaffold. Video-watching activity is mostly coupled to the structure across the whole brain. Regions exhibiting the strongest coupling are the Primary Somatosensory cortex (Area 2; SDI: -1.8), Primary Sensory cortex (SDI: -1.8) and Second Visual area (V2; SDI: -1.8). Activities from the regions such as the Parahippocampal Area 2 (SDI: 0.62), Inferior Frontal Sulcal area (IFJp; SDI: 0.5), and Posterior parietal cortex (Area 5L; SDI: 0.2) are decoupled from the underlying anatomy. We also investigated temporal dynamics of coupling over specific periods in the video and found that the SDI was not different between moments of strongest and weakest intersubject correlation (see supplementary material, Fig 6).

The group-level SDI map for the rest condition is displayed in Fig 2d. During resting-state, EEG is mostly coupled to the structural graph, similarly to the video. Notably, primary somatosensory cortex (BA1, SDI: -1.78), Visual V2, and V3 (SDI: -1.74 each) exhibited strong coupling, whereas the Parahippocampal area 2 (SDI: 0.71), Inferior Frontal Sulcal area (IFJp; SDI: 0.6), and Subgenual Anterior Cingulate cortex (Area s32; SDI: 0.38) showed decoupling from the structure. While some effects appear to be specific to video-watching tasks, most patterns appear to be consistent between rest and video-watching.

3.2 Stronger coupling to the structure while watching movie as compared to rest

To further investigate the differences between video and resting state, we compared the SDI in the two conditions (Fig 2e). The statistical comparison (Paired t-test, FDR-corrected at $\alpha = 0.05$) revealed differences in the coupling relationship between video and rest. Note that these are to be interpreted as weaker coupling (red), and stronger coupling (blue) during movie-watching relative to resting state. Regions that exhibit stronger coupling during video watching as compared to rest were found to be widespread across the whole brain. In particular, stronger coupling was observed in the Visual area 7 (V7; t(42) = -5), Inferior parietal cortex (Area PGP; t(42) = -4.65) and Middle temporal area (t(42)

= -4.64) during movie-watching. No region exhibited weaker coupling. Wideband EEG is tethered consistently within condition during video and the relationship is strengthened during movie. Given this observation, one may wonder whether the coupling relationship of the EEG frequency bands could exhibit a distinct behavior.

3.3 Structure-Function relationships are similar across EEG frequency bands

We investigated whether all EEG frequency bands (cortical envelopes) are related to the underlying anatomical structure in the same way through an analysis focused on each of the EEG frequency bands i.e θ (4 - 8Hz), α (8 - 13Hz), Low β (13 - 20Hz), High β (20 - 30Hz), γ (30 - 40Hz). Results are presented in the first four columns of Fig 3. Upon closer examination of the SDI values specifically for the regions such as the Retroinsular cortex (Mean SDI: -1.2, σ: 0.1), Primary Auditory Cortex (Mean SDI: -1.1, σ: 0.2) exhibited consistent coupling, whereas the Parahippocampal area (Mean SDI: 0.8, σ: 0.07) exhibited consistent decoupling across frequency bands. We compared the coupling relationship between video and rest for the specific EEG frequency bands. Results (presented in the last column of Fig 3) revealed that the stronger coupling observed during movie-watching in areas such as Retrosplenial complex and Motor cortices still holds for different EEG frequency bands.

We further investigated how the SDIs are related across frequency bands by computing the Spearman's correlation coefficient in 7 Yeo-Krienen networks. Results showed a significant correlation across all EEG frequencies and in all seven networks (average $\rho = 0.93$, all p-values $< 10^{-7}$).

3.4 SDI spatial maps are consistent across two different videos

We investigated the test-retest reliability of our study's findings with Video 2. We performed a reliability analysis on a mean rating (raters corresponding to the two videos) with a two-way random-effects model. Our analysis revealed that the ICC estimates is 0.83 and the 95% CI is [0.79, 0.86] for the said parameters, indicating a good degree of reliability across videos. Furthermore, we ran a reliability analysis on the SDI contrasts between rest and Video (rater 1 = Video 1 vs Rest; rater 2 = Video 2 vs Rest). Our findings revealed that the ICC estimates were 0.68, and the 95% CI was [0.6, 0.75], indicating a good amount of reliability in contrast between video and rest. We also assessed the extent of agreement between task conditions by computing ICC coefficients for either of the videos and rest. The results revealed that the ICC was 0.79 and the 95% CI was [0.75, 0.83] when comparing video 1 with rest and the ICC was 0.78 and the 95% CI was [0.73, 0.82] with the video 2. Taken all the pairs of ICC tests together, we can

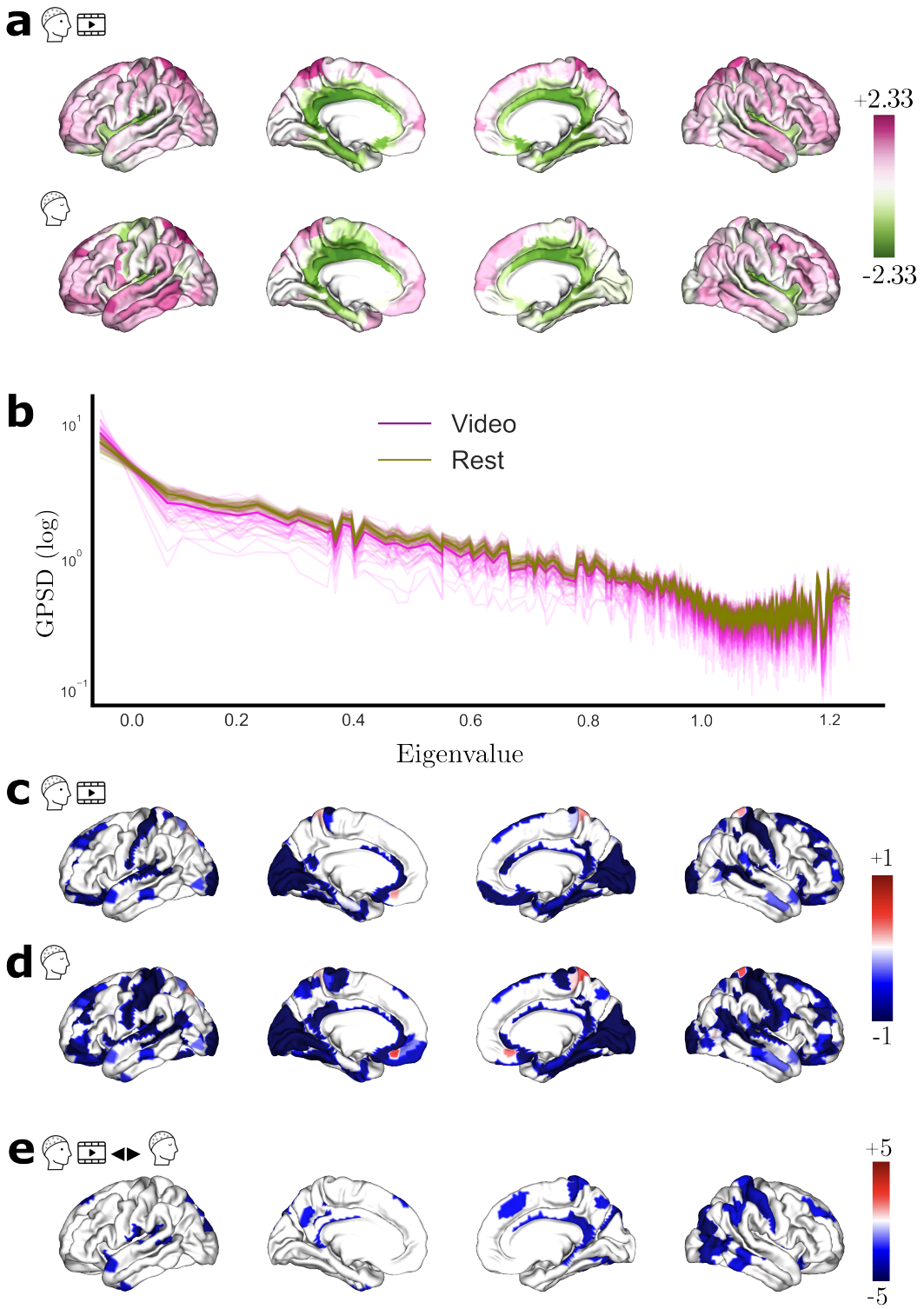

Figure 2: Source-localized EEG and SDI maps. **a** Averaged cortical activity (in zscore) for Video 1 (top row) and resting-state. **b** Averaged graph PSD for all subjects (magenta - Video 1; olive - Rest). The power spectrum is in log scale, displayed as a function of consensus structural graph eigenvalues. **c** Group level SDI maps (using subject-specific structural connectome) for Video 1 and **d** for Rest. For visualization purposes only, and due to the log scale of SDI, values are clipped to -1 / +1. **e** SDI contrast t-values maps (FDR corrected) resulting from the statistical comparison between Video 1 and Rest, with blue (and red) denoting stronger (and weaker) coupling during the movie than during rest

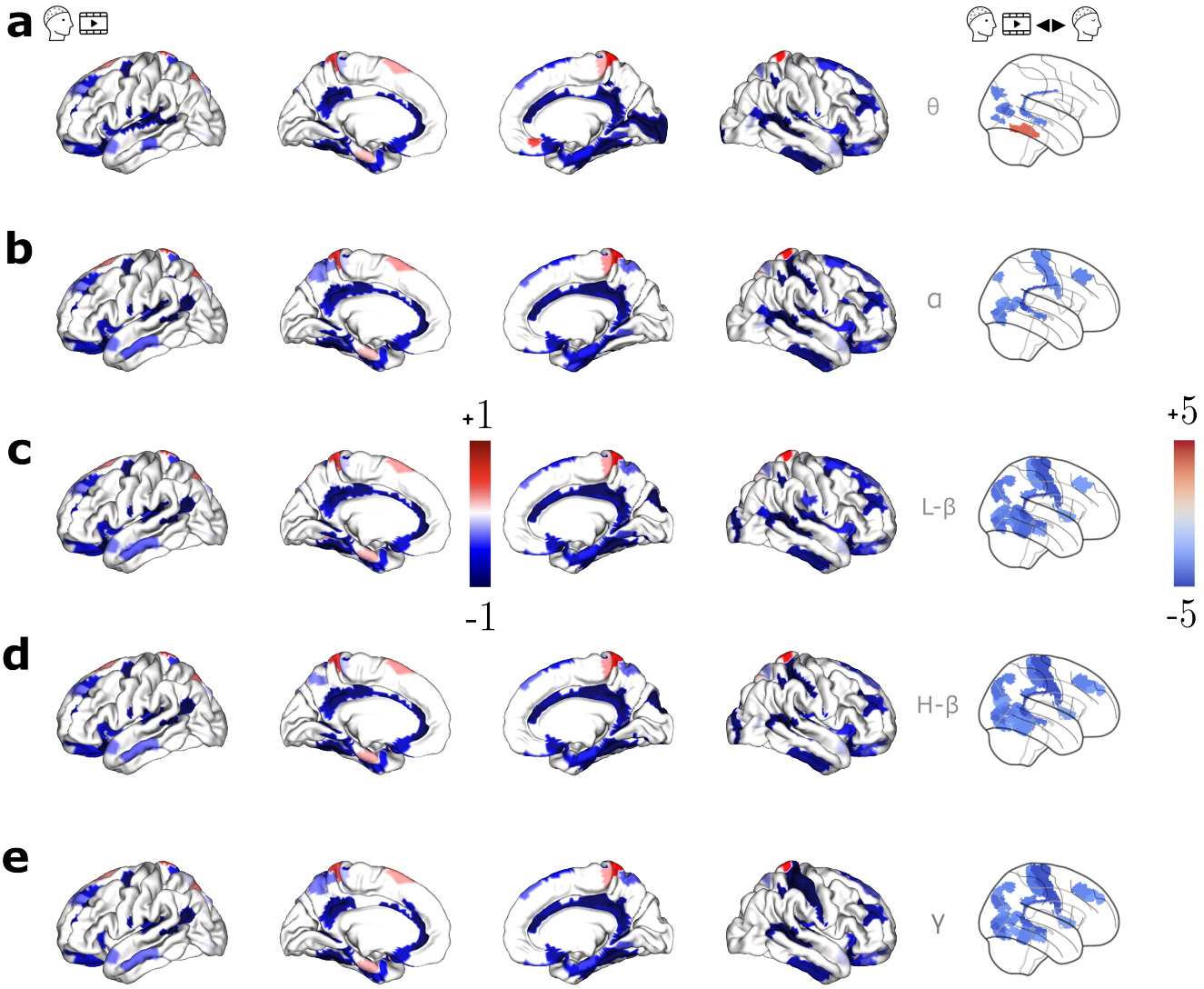

Figure 3: Group SDI maps during video watching (Video 1) in different EEG frequency bands: **a** θ (4-7Hz), **b** α (8-13Hz), **c** Low β (13-20Hz), **d** High β (20-30Hz), and **e** γ (30-40Hz). The first four columns display group-level significant SDI maps, with red and blue indicating respectively decoupling and coupling. The last column shows the group-level SDI contrast t-values maps (FDR corrected) resulting from the statistical comparison between Video 1 and Rest, with red (and blue) denoting weaker (and stronger) coupling during the movie than during rest

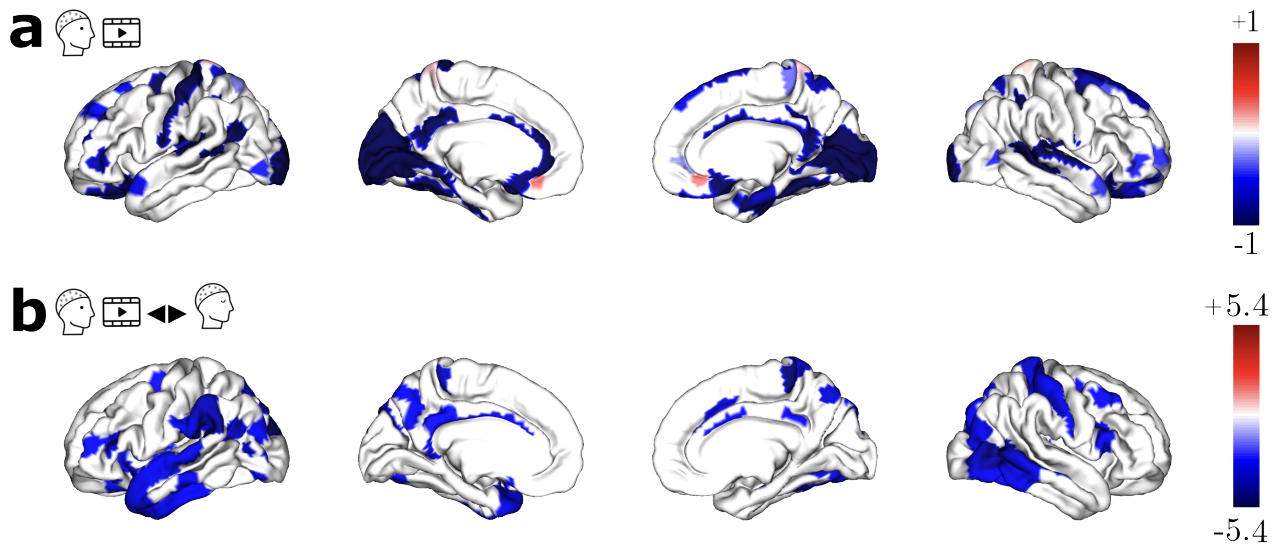

Figure 4: Structure-Function relationship for Video 2. **a** Group-level SDI map for Video 2. **b** SDI contrast t-values maps (FDR corrected) resulting from the statistical comparison between Video 2 and Rest, with red (and blue) denoting weaker (and stronger) coupling during the movie than during rest

observe the agreement between videos was higher than the agreement between distinct task conditions, suggesting the topography is more similar between videos than between videos and rest.

Fig 4 shows SDI maps corresponding to video 2 (Fig 4a), and contrast between video 2 and resting state (Fig 4b), both FDR-corrected at $\alpha = 0.05$. As with Fig 2e, the blue tail in Fig 4b indicates stronger coupling during video 2 compared to the resting state. Our results revealed that the regions such as Visual areas (V3A, V6A; t(42) = -5.4, -5.4 respectively) and primary somatosensory cortex (Area 5m; t(42) = -5.2) exhibited stronger coupling during movie. Overall, the trend was largely similar to the results obtained for video 1 (Fig 2e).

3.5 Functional decoding of the structure-function relationship

We performed functional decoding of SDI spatial maps with a meta-analytic search of brain maps and associated topics terms in the literature. The results for decoding the wideband SDI maps are presented in Fig 5. Panels a) and c) show the results for Video 1 and 2, while panel b) shows the results for the resting state. The thresholded spatial maps are shown in the first column as a reference and the second column displays the decoding results. The unthresholded spatial maps that were used to perform decoding are presented in both sides of the colorbar. The arrangement can be thought of as a strong coupling-weak coupling gradient, where the ascending order indicates more untethering from the underlying structure.

SDI maps were binned at 10%ile increments, and decoding was performed for these 10 "activations maps". The lower percentiles indicate strong coupling to the underlying structure (corresponding spatial map on the left side of the colorbar), whereas the higher percentiles correspond to weaker coupling (corresponding spatial map on the right side of the colorbar). Our decoding analysis of the spatial map for both Video 1 and Rest revealed that the unimodal visual systems and motor systems were associated with strong coupling (0 to 40th percentiles in Fig 5a and 5b, topics highlighted in yellow). Though the other unimodal system Auditory is associated to coupling, this system can be observed to be relatively flexible extending between 20th to 90th percentile. Results obtained for Video 2 (Fig 5c) indicate a closer similarity to Video 1 than to rest, with the key difference being that during rest the correlation of the auditory system was also found around the coupling-decoupling divergence. However, higher-order systems such as mental imagery, emotions, and memory retrieval / encoding (Fig 5, topics highlighted in pink) were more distributed across the strong coupling-weak coupling gradient, similarly in Video 1, Rest and Video 2.

4 Discussion

The static anatomical scaffold in the brain gives rise to complex and dynamic functions ranging from primary perceptual tasks to higher-order cognitive processes (Honey et al., 2009; Park & Friston, 2013; Pascucci, Rubega, et al., 2022; Tewarie et al., 2019). Here, we studied how brain activity is coupled to the underlying anatomy, by analyzing how the source-localized EEG is linked to structural connectivity (derived from individual DWI data) during movie-watching and during rest. A Graph Signal Processing framework (Preti & Van De Ville, 2019) was sought out to quantify structure-function coupling. In particular, the eigenvectors of individual structural graph Laplacians were used to define a Graph Fourier Transform and isolate low and high graph-frequency components. The association between structure-function was then quantified using the SDI, calculated as a ratio between low- and high graph-frequency components of the brain activity (Preti & Van De Ville, 2019). In the following discussion of the results, we interchangeably use the terms "weaker coupling" and "decoupling" when referring to the results of this study.

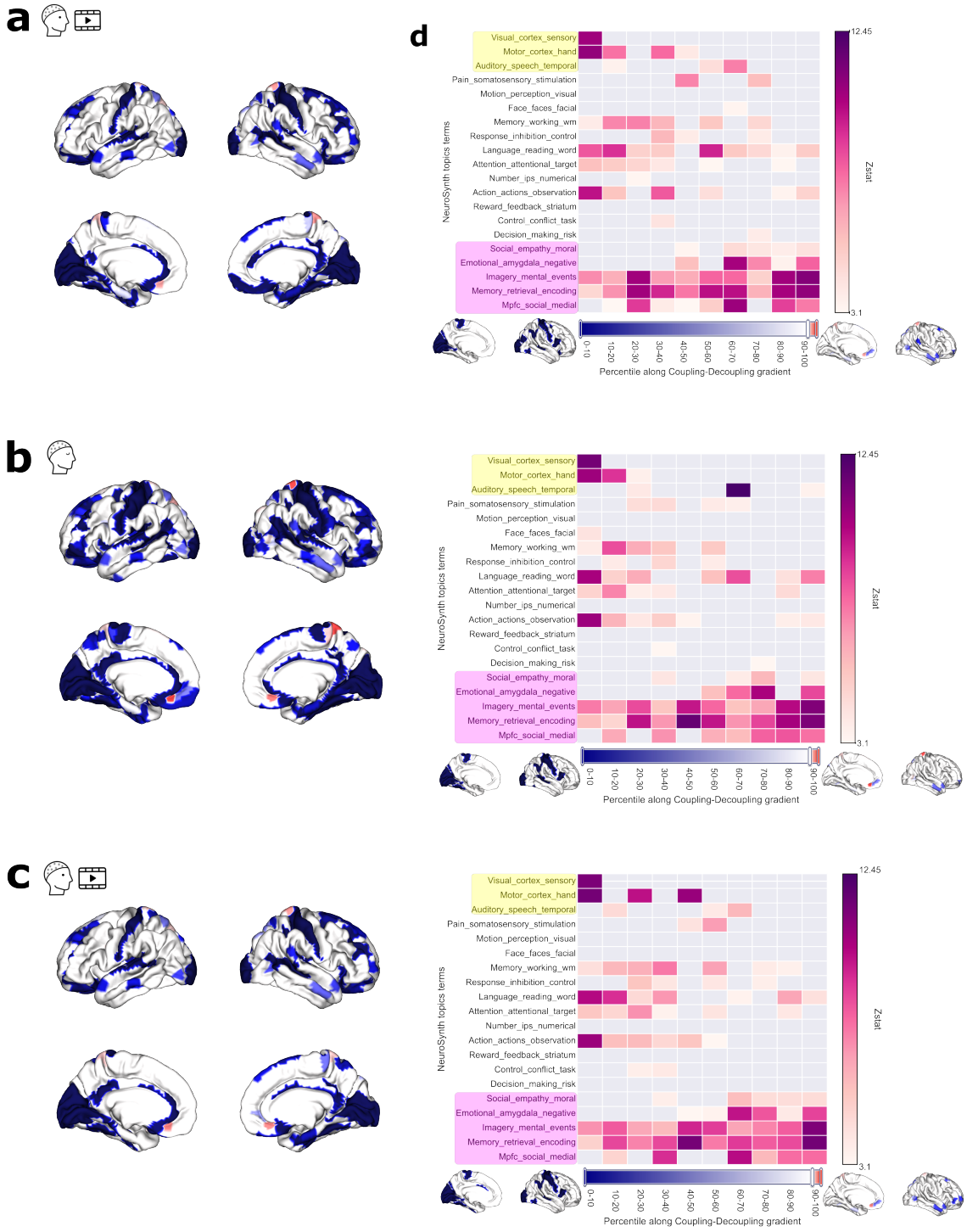

Figure 5: Results of the Neurosynth meta-analysis of SDI maps for **a** Video 1, **b** Rest and **c** Video 2. Decoding results, shown as thresholded z statistics as a function of topic terms, are reported on the right as a function of percentile along the decoupling index gradient (i.e. binned SDI values). Yellow and pink topic terms correspond to unimodal and transmodal systems respectively, following the convention used in Preti and Van De Ville, 2019. The unthresholded maps, corresponding to first and last decile bins, used to perform decoding are presented on the sides of the colorbar. The color of the horizontal colorbar corresponds to coupling in blue, and decoupling in red. The corresponding thresholded group-level SDI spatial maps are reported on the left.

4.1 EEG in sensory areas is coupled to structural connectivity in movie-watching and resting state

A limited number of studies have undertaken the joint analysis of EEG cortical activity with structural connectomes using GSP, either with visual event-related potentials (Glomb et al., 2020; Rué-Queralt et al., 2021), auditory steady-state responses (Rué-Queralt et al., 2023) or during interictal epileptic discharges (Rigoni et al., 2023). Because the focus in these studies was on event-related experiments, the probed time windows were brief, ranging from a few hundred milliseconds to a few seconds. By contrast, our study investigates structure-function coupling with several minutes of continuous EEG and individual structural connectomes. Our findings (Fig 2c-d, Fig 5) indicate that the wideband activity in visual, motor and auditory systems are coupled to the underlying structure across Video 1, 2, and Rest. These observations confirm and extend previous research (Glomb et al., 2020; Rué-Queralt et al., 2021, 2023), which has evaluated the contribution of structural connectivity eigenmodes in expressing the cortical EEG during visual and auditory tasks. Their observation that the sparse set of eigenmodes suffices to reconstruct the source activity implies that the low-frequency eigenmodes carry more signal power (i.e., more expressive) relative to their high-frequency counterpart. By definition of the SDI metric, this refers to coupling. Studies such as Glomb et al., 2020; Rué-Queralt et al., 2021 found that during visual-evoked tasks, the signal becomes more compact, i.e., the first few eigenmodes capture most of the signal power. In particular, Rué-Queralt et al., 2021, 2023 found that during visual and auditory tasks, the contributions of the low-frequency eigenmodes become dominant, also indicating coupling during the said tasks. As a consequence, our findings in sensory regions during continuous, long EEG segments complement the observations during isolated, shorter events, suggesting a consistent behavior of these systems during short and long time periods. In addition, existing work has estimated SDI with MEG during resting state, and also found that visual regions (among others) were strongly coupled to the structural connectome (Griffa & Preti, 2022).

From the individual analysis with distinct continuous cognitive states such as video and rest, we observed a largely similar trend consistently across cognitive states. This prompted a question whether the coupling relationship reorganizes selectively depending on task. To this end, we analyzed the coupling relationship between video and rest through a pairwise comparison. Results (Fig 2e) indicated that the wideband activity during the movie exhibits stronger coupling across the cortex. In particular, late visual areas such as V3, V6, and somatosensory cortex exhibit stronger coupling during the movie, a trend consistent across both videos. This observation goes inline with the prior studies such as (Glomb et al., 2020; Rué-Queralt et al., 2021) in terms of more coupling during visual-evoked events relative to moments prior. Taken together, while the coupling relationship of the sensory systems is largely stable across

cognitive states, the strength of the structure-function in selected systems appears to be modulated by the ongoing task condition.

4.2 Decoupling of EEG activity in parahippocampal and inferior frontal areas

We found that the parahippocampal area and inferior frontal areas were decoupled with the structure, a trend consistent across videos and during rest. In a study from Rigoni and colleagues analyzing EEG during four second-long epochs of interictal epileptic spikes decomposed on network harmonics (i.e. eigenvectors) of a structural connectome, the authors report that at least three patients have significant decoupling of ventral, parahippocampal areas as well as inferior frontal areas (Rigoni et al., 2023). In addition, prior work using resting-state MEG on 84 subjects have found the same regions to be decoupled according to the SDI (Griffa & Preti, 2022). Taken together, these results suggest decoupling of similar brain areas from short periods of four seconds in Rigoni's study (Rigoni et al., 2023), and up to a few minutes of resting state and video watching in our results and in Griffa and Preti's (Griffa & Preti, 2022). This questions the potential presence of time-varying aspects of structure-function coupling.

4.3 Temporal stability of structure-function coupling during video watching

To investigate whether the relationship varies within conditions (i.e. within video), we assessed the coupling relationship at a temporally localized segment, by selecting moments of high correlation of cortical activity across subjects (Strong ISC). Such Strong ISC periods correspond to when brain activity is most correlated across subjects watching the same movie. Hasson et al., 2004 has pioneered this line of work investigating the shared neural response evoked by audiovisual stimuli. Here we extend the investigation further by analyzing the structure-function relationship of the correlated activity. We examined whether the salient events in the movie could modulate the dynamics of structure-function relationship and we found that the coupling relationship during Strong ISC periods does not statistically differ from what was observed during Weak ISC periods (supplementary Fig 6). We also did not find any differences when comparing SDI values from a pair of random segments during the video, suggesting that SDI does not capture time-varying aspects of structure-function coupling.

4.4 Similarity of structure-function coupling across EEG frequency bands

We also analyzed whether the SDI patterns differ across distinct EEG frequency bands (Fig 3, first four columns), and observed a strong correlation in the SDI values between frequency bands, suggesting consistency of the coupling relationship across frequency bands. Prior research on MEG data at rest (Griffa & Preti, 2022) observed a similar trend across δ to β bands. Comparing between conditions, regions such as the motor cortices and Retrosplenial complex in the PCC exhibited stronger coupling to the structure during the movie across all frequency bands (Fig 3 last column). In Rué-Queralt et al., 2023, the authors defined a joint transform over graph and frequency domain by combining structural harmonics with Morlet wavelets (called "time vertex spectral representation" in their paper), and applied to EEG in visual and auditory tasks. They found that slower EEG rhythms were mostly coupled to the structure, while the activity of faster temporal frequencies tended to be more decoupled (Rué-Queralt et al., 2023). In contrast, we found regions such as parahippocampus, inferior frontal junction to be consistently decoupled across slow and fast EEG rhythms during several minutes of EEG. This difference might arise from the variation in window duration, which was around a few seconds in Rué-Queralt et al., 2023, compared to substantially longer durations in our study and in Griffa and Preti's study (Griffa & Preti, 2022).

4.5 Spatially focal coupling relationship in higher-order systems compared to haemodynamics

Here we relate the coupling relationship of the EEG SDI results with the existing work analyzing haemodynamic responses, to assess the possibility of a similar structure-function coupling at two distinct temporal scales. The question of whether the coupling relationship of the brain response at a slower time scale (e.g: haemodynamic) and the electrophysiological response exhibit an overlapping trend has not been fully studied before. One study from Griffa and Preti (Griffa & Preti, 2022) with MEG data showed that the group-averaged SDI patterns deviated from studies with fMRI (Preti & Van De Ville, 2019). Numerous studies have shown and confirmed the global hierarchy from unimodal-transmodal in different contexts, ranging from cortical microstructure (Huntenburg et al., 2017), to macroscale connectivity (Bernhardt et al., 2022; Margulies et al., 2016) and structure-function coupling (Preti & Van De Ville, 2019)(see Huntenburg et al., 2018 for a review). Our findings (Fig 5) show that the cortical activity in the sensorimotor areas during both videos and rest is generally coupled to the structure, supporting prior research. In particular, studies such as (Margulies et al., 2016; Preti & Van De Ville, 2019; Yang et al., 2023) analyzed the macroscale organization or the coupling relationship using resting-state fMRI, and

generally found a gradient-like spatial organisation from sensorimotor systems to transmodal ones. Preti and Van de Ville (Preti & Van De Ville, 2019) observed that the three systems exhibiting strong coupling include Visual, Motor, and Auditory, and some of the systems exhibiting strong decoupling include Emotion, Social Cognition, and Memory. Situating these systems in the context of EEG reveals that they are very much in agreement not only at Rest but also during both videos, and a similar pattern was found in MEG (Griffa & Preti, 2022). However, there are two key differences in our functional decoding results (Fig 5). The first one is the relative place of the auditory system, which was less coupled than the motor and visual systems, in both Rest and Video, which suggests flexibility in the coupling of the auditory system with respect to the structure. Additionally, transmodal systems such as Social, Memory-retrieval, and Emotion were associated in our EEG results with a wider range of structure-function patterns ranging from strongly coupled to weakly coupled areas. Taken together, our results with EEG confirm previous observations with fMRI in the sensorimotor cortex, while it contributes to understanding more about the dynamics of EEG in the transmodal cortices, with the spatially refined structure-function relationship.

4.6 The topography of EEG structure-function coupling is consistent across movie-watching and resting-state

Movies can elicit a richer repertoire of brain states than resting-state, providing a window to understand both exteroceptive and interoceptive processes (Meer et al., 2020). Whether the cortical organization during the movie differs from the resting state has been previously studied (Kringelbach et al., 2023; Samara et al., 2023). For example, Samara et al. 2023 show that cortical organization during movie-watching follows a different principle than during rest, with the gradients being modality-specific. They found that during movie-watching the default mode network and frontoparietal network formed a heteromodal peak, while the sensorimotor regions anchored the unimodal pole for the first three fMRI gradients. Another fMRI study from Kringelbach and colleagues (Kringelbach et al., 2023) investigated the hierachical reorganisation of the functional brain activity during movie compared to rest, using a generative model of effective connectivity. This approach enables to model the direction of information flow, and estimate the hierarchy of activity as a change of balance in causal interactions between brain regions, under different task conditions of movies and rest. Their findings indicate that fMRI activity is relatively less hierarchical during movie than during rest, as they beautifully put it as "flattening of the hierarchy". This sparks the question as to whether the coupling relationship is also reshaped between movie and rest. While there is no study directly comparing structure-function coupling in fMRI using both resting-state and video watching, our findings using EEG suggests a similar spatial distribution of coupling across tasks. Specifically, sensory systems strongly coupled to the structure are apparent across

all contexts, while the coupling relationship in the higher-order systems is flattened as during rest (i.e. from coupling to decoupling, Fig 5). When perfoming a pairwise comparison between movie and rest however, we found the coupling relationship was strengthened watching a movie.

4.7 Limitations and perspectives

Several limitations need to be acknowledged, as they may be useful to consider in follow-up research building on our work. Firstly, we have used a template for the spatial definition of ROIs, using the HCP-MMP atlas (Glasser et al., 2016), known to have a good generalization across subjects. However, results might differ when using individually defined parcels or hyper-alignment methods (Xu et al., 2012; Zhou et al., 2022). This aspect could be the subject of future work, in particular with datasets that are adapted to estimate individual parcellations and connectomes (Pascucci, Tourbier, et al., 2022). Secondly, we did not find any temporal specificity in structure-function coupling when investigating peaks of ISC. While ISC attempts to identify neural correlates of naturalistic perception with a data-driven approach, an alternative approach to investigate time-varying aspects could be to predict structure-function coupling directly using stimulus features, similar to how an encoding model predicts brain activity from the stimulus (Holdgraf et al., 2017; Yamins et al., 2014). Finally, we were unable to show clear differences in the topography of the SDI pattern as a function of classical EEG frequency bands. An interesting perspective could revisit this result by reparameterizing the EEG power spectrum using aperiodic and periodic components (Donoghue et al., 2020).

4.8 Conclusions

In this study, we provide a comprehensive charaterization of the structure-function relationship based on diffusion imaging and cortical EEG recorded while participants either rested or watched a movie. We quantified the coupling patterns using subject-specific Eigenmodes of individual structural connectomes using graph signal processing. Our findings suggest a similar spatial topography of coupling of sensory systems to the structure across video watching and rest, complementing prior results obtained with fMRI. We also found a few regions to be consistently decoupled from the structure, namely the parahippocampal cortex and superior parietal areas, and an overall strengthening of coupling in movie watching compared to resting-state. Our results obtained with continuous EEG (several minutes of movie-watching and rest) also bring complementary insights with respect to previous work that has analyzed the link between EEG and structural connectivity during event-related short data segments. While the coupling relationship was consistent between videos and across slower and faster EEG rhythms, the said relationship was not

significantly different within video during periods of strong inter-subject correlation. Using functional decoding we showed that the cortical activity in the unimodal systems were associated to strong coupling, inline with previous fMRI findings, whereas the higher-order systems such as memory retrieval and emotions were associated between coupling and decoupling, bringing in novel insights compared to previous fMRI work.

5 CRediT Statement

Venkatesh Subramani: Conceptualization, Methodology, Software, Validation, Formal Analysis, Investigation, Writing - Original Draft, Writing - Review & Editing, Visualization. **Giulia Lioi**: Conceptualization, Methodology, Resources, Writing - Review & Editing, Supervision, Project administration. **Karim Jerbi**: Conceptualization, Writing - Review & Editing, Supervision, Project administration. **Nicolas Farrugia**: Conceptualization, Methodology, Resources, Writing - Review & Editing, Supervision, Project administration.

6 Conflict of Interest Statement

The authors declare no competing interest.

7 Code and Data availability

All the scripts necessary to perform analysis are shared on Github

8 Acknowledgements

EEG and DWI data were shared as part of the Healthy Brain Network. We thank Maxmillian Nentwich for providing us the list of subjects having good quality EEG identified in their study (Nentwich et al., 2020). We are grateful to Maria-Giulia Preti for sharing us the details about the pipeline utilized in their study (Preti & Van De Ville, 2019) for constructing structural connectome. Our Qsiprep pipeline was run in a High-Performance Cluster grid thanks to the BC DRI Group, Calcul québec and the Digital Research Alliance of Canada (https://alliancecan.ca/) and we appreciate their continued support and swift action

in fixing a problem during the analysis. We also thank Alix Lamouroux for helping us get started with Qsiprep, and Yassine El Ouahidi for providing us the script to perform decoding with NiMare.

K.J. is supported by funding from the Canada Research Chairs (950-232368) program and a Discovery Grant from the Natural Sciences and Engineering Research Council of Canada (2021-03426).

References

Atasoy, S., Donnelly, I., & Pearson, J. (2016). Human brain networks function in connectome-specific harmonic waves. *Nature communications*, *7*(1), 10340.

Bajada, C. J., Costa Campos, L. Q., Caspers, S., Muscat, R., Parker, G. J., Lambon Ralph, M. A., Cloutman, L. L., & Trujillo-Barreto, N. J. (2020). A tutorial and tool for exploring feature similarity gradients with MRI data. *NeuroImage*, *221*(January), 117140. https://doi.org/10.1016/j.neuroimage.2020.117140

Bassett, D. S., & Sporns, O. (2017). Network neuroscience. *Nature neuroscience*, *20*(3), 353–364.

Bernhardt, B. C., Smallwood, J., Keilholz, S., & Margulies, D. S. (2022). Gradients in brain organization. *NeuroImage*, *251*, 118987.

Cieslak, M., Cook, P. A., He, X., Yeh, F.-C., Dhollander, T., Adebimpe, A., Aguirre, G. K., Bassett, D. S., Betzel, R. F., Bourque, J., et al. (2021). Qsiprep: An integrative platform for preprocessing and reconstructing diffusion mri data. *Nature methods*, *18*(7), 775–778.

Dhollander, T., Mito, R., Raffelt, D., & Connelly, A. (2019). Improved white matter response function estimation for 3-tissue constrained spherical deconvolution. *Proc. Intl. Soc. Mag. Reson. Med*, *555*(10).

Dmochowski, J. P., Sajda, P., Dias, J., & Parra, L. C. (2012). Correlated components of ongoing eeg point to emotionally laden attention–a possible marker of engagement? *Frontiers in human neuroscience*, *6*, 112.

Donoghue, T., Haller, M., Peterson, E. J., Varma, P., Sebastian, P., Gao, R., Noto, T., Lara, A. H., Wallis, J. D., Knight, R. T., et al. (2020). Parameterizing neural power spectra into periodic and aperiodic components. *Nature neuroscience*, *23*(12), 1655–1665.

Faskowitz, J., Moyer, D., Handwerker, D. A., Gonzalez-Castillo, J., Bandettini, P. A., Jbabdi, S., & Betzel, R. (2023). *Commentary on pang et al. (2023)nature*. https://doi.org/10.1101/2023.07.20.549785

Fischl, B. (2012). Freesurfer. *Neuroimage*, *62*(2), 774–781.

Glasser, M. F., Coalson, T. S., Robinson, E. C., Hacker, C. D., Harwell, J., Yacoub, E., Ugurbil, K., Andersson, J., Beckmann, C. F., Jenkinson, M., et al. (2016). A multi-modal parcellation of human cerebral cortex. *Nature*, *536*(7615), 171–178.

Glomb, K., Kringelbach, M. L., Deco, G., Hagmann, P., Pearson, J., & Atasoy, S. (2021). Functional harmonics reveal multi-dimensional basis functions underlying cortical organization. *Cell Reports*, *36*(8).

Glomb, K., Queralt, J. R., Pascucci, D., Defferrard, M., Tourbier, S., Carboni, M., Rubega, M., Vulliemoz, S., Plomp, G., & Hagmann, P. (2020). Connectome spectral analysis to track eeg task dynamics on a subsecond scale. *NeuroImage*, *221*, 117137.

Gramfort, A., Luessi, M., Larson, E., Engemann, D. A., Strohmeier, D., Brodbeck, C., Goj, R., Jas, M., Brooks, T., Parkkonen, L., & Hämäläinen, M. S. (2013). MEG and EEG data analysis with MNE-Python. *Frontiers in Neuroscience*, *7*(267), 1–13. https://doi.org/10.3389/fnins.2013.00267

Griffa, A., & Preti, M. G. (2022). Brain structure-function coupling is unique to individuals across multiple frequency bands: A graph signal processing study. *2022 30th European Signal Processing Conference (EUSIPCO)*, 942–946.

Hagmann, P., Cammoun, L., Gigandet, X., Meuli, R., Honey, C. J., Wedeen, V. J., & Sporns, O. (2008). Mapping the structural core of human cerebral cortex. *PLoS biology*, *6*(7), e159.

Hasson, U., Nir, Y., Levy, I., Fuhrmann, G., & Malach, R. (2004). Intersubject synchronization of cortical activity during natural vision. *science*, *303*(5664), 1634–1640.

Holdgraf, C. R., Rieger, J. W., Micheli, C., Martin, S., Knight, R. T., & Theunissen, F. E. (2017). Encoding and decoding models in cognitive electrophysiology. *Frontiers in systems neuroscience*, *11*, 61.

Honey, C. J., Sporns, O., Cammoun, L., Gigandet, X., Thiran, J.-P., Meuli, R., & Hagmann, P. (2009). Predicting human resting-state functional connectivity from structural connectivity. *Proceedings of the National Academy of Sciences*, *106*(6), 2035–2040.

Huntenburg, J. M., Bazin, P.-L., Goulas, A., Tardif, C. L., Villringer, A., & Margulies, D. S. (2017). A systematic relationship between functional connectivity and intracortical myelin in the human cerebral cortex. *Cerebral Cortex*, *27*(2), 981–997.

Huntenburg, J. M., Bazin, P.-L., & Margulies, D. S. (2018). Large-scale gradients in human cortical organization. *Trends in cognitive sciences*, *22*(1), 21–31.

Koo, T. K., & Li, M. Y. (2016). A guideline of selecting and reporting intraclass correlation coefficients for reliability research. *Journal of chiropractic medicine*, *15*(2), 155–163.

Kringelbach, M. L., Perl, Y. S., Tagliazucchi, E., & Deco, G. (2023). Toward naturalistic neuroscience: Mechanisms underlying the flattening of brain hierarchy in movie-watching compared to rest and task. *Science Advances*, *9*(2), eade6049.

Langer, N., Ho, E. J., Alexander, L. M., Xu, H. Y., Jozanovic, R. K., Henin, S., Petroni, A., Cohen, S., Marcelle, E. T., Parra, L. C., et al. (2017). A resource for assessing information processing in the developing brain using eeg and eye tracking. *Scientific data*, *4*(1), 1–20.

Lioi, G., Gripon, V., Brahim, A., Rousseau, F., & Farrugia, N. (2021). Gradients of connectivity as graph fourier bases of brain activity. *Network Neuroscience*, *5*(2), 322–336.

Lynn, C. W., & Bassett, D. S. (2019). The physics of brain network structure, function and control. *Nature Reviews Physics*, *1*(5), 318–332.

Margulies, D. S., Ghosh, S. S., Goulas, A., Falkiewicz, M., Huntenburg, J. M., Langs, G., Bezgin, G., Eickhoff, S. B., Castellanos, F. X., Petrides, M., et al. (2016). Situating the default-mode network along a principal gradient of macroscale cortical organization. *Proceedings of the National Academy of Sciences*, *113*(44), 12574–12579.

Medaglia, J. D., Lynall, M.-E., & Bassett, D. S. (2015). Cognitive network neuroscience. *Journal of cognitive neuroscience*, *27*(8), 1471–1491.

Meer, J. N. v. d., Breakspear, M., Chang, L. J., Sonkusare, S., & Cocchi, L. (2020). Movie viewing elicits rich and reliable brain state dynamics. *Nature communications*, *11*(1), 5004.

Nentwich, M., Ai, L., Madsen, J., Telesford, Q. K., Haufe, S., Milham, M. P., & Parra, L. C. (2020). Functional connectivity of eeg is subject-specific, associated with phenotype, and different from fmri. *NeuroImage*, *218*, 117001.

Pang, J. C., Aquino, K. M., Oldehinkel, M., Robinson, P. A., Fulcher, B. D., Breakspear, M., & Fornito, A. (2023a). Geometric constraints on human brain function. *Nature*, 1–9.

Pang, J. C., Aquino, K. M., Oldehinkel, M., Robinson, P. A., Fulcher, B. D., Breakspear, M., & Fornito, A. (2023b). Reply to: Commentary on pang et al.(2023) nature. *bioRxiv*, 2023–10.

Paquola, C., Vos De Wael, R., Wagstyl, K., Bethlehem, R. A., Hong, S. J., Seidlitz, J., Bullmore, E. T., Evans, A. C., Misic, B., Margulies, D. S., Smallwood, J., & Bernhardt, B. C. (2019). Microstructural and functional gradients are increasingly dissociated in transmodal cortices. *PLoS Biology*, *17*(5), 1–28. https://doi.org/10.1371/journal.pbio.3000284

Park, H.-J., & Friston, K. (2013). Structural and functional brain networks: From connections to cognition. *Science*, *342*(6158), 1238411.

Parra, L. C., Haufe, S., & Dmochowski, J. P. (2018). Correlated components analysis-extracting reliable dimensions in multivariate data. *arXiv preprint arXiv:1801.08881*.

Pascual-Marqui, R. D., Lehmann, D., Koukkou, M., Kochi, K., Anderer, P., Saletu, B., Tanaka, H., Hirata, K., John, E. R., Prichep, L., et al. (2011). Assessing interactions in the brain with exact low-resolution electromagnetic tomography. *Philosophical Transactions of the Royal Society A: Mathematical, Physical and Engineering Sciences*, *369*(1952), 3768–3784.

Pascucci, D., Rubega, M., Rué-Queralt, J., Tourbier, S., Hagmann, P., & Plomp, G. (2022). Structure supports function: Informing directed and dynamic functional connectivity with anatomical priors. *Network Neuroscience*, *6*(2), 401–419.

Pascucci, D., Tourbier, S., Rué-Queralt, J., Carboni, M., Hagmann, P., & Plomp, G. (2022). Source imaging of high-density visual evoked potentials with multi-scale brain parcellations and connectomes. *Scientific Data*, *9*(1), 9.

Patil, K. R., Jung, K., & Eickhoff, S. B. (2023). Commentary on pang et al.(2023) nature. *bioRxiv*, 2023–10.

Pirondini, E., Vybornova, A., Coscia, M., & Van De Ville, D. (2016). A spectral method for generating surrogate graph signals. *IEEE signal processing letters*, *23*(9), 1275–1278.

Preti, M. G., & Van De Ville, D. (2019). Decoupling of brain function from structure reveals regional behavioral specialization in humans. *Nature communications*, *10*(1), 4747.

Rigoni, I., Queralt, J. R., Glomb, K., Preti, M., Roehri, N., Tourbier, S., Spinelli, L., Seeck, M., Van De Ville, D., Hagmann, P., et al. (2023). Structure-function coupling increases during interictal spikes in temporal lobe epilepsy: A graph signal processing study. *Clinical Neurophysiology*.

Rué-Queralt, J., Glomb, K., Pascucci, D., Tourbier, S., Carboni, M., Vulliémoz, S., Plomp, G., & Hagmann, P. (2021). The connectome spectrum as a canonical basis for a sparse representation of fast brain activity. *NeuroImage*, *244*, 118611.

Rué-Queralt, J., Mancini, V., Rochas, V., Latrèche, C., Uhlhaas, P. J., Michel, C. M., Plomp, G., Eliez, S., & Hagmann, P. (2023). The coupling between the spatial and temporal scales of neural processes revealed by a joint time-vertex connectome spectral analysis. *NeuroImage*, *280*, 120337.

Salo, T., Yarkoni, T., Nichols, T. E., Poline, J.-B., Kent, J. D., Gorgolewski, K. J., Glerean, E., Bottenhorn, K. L., Bilgel, M., Wright, J., Reeders, P., Kimbler, A., Nielson, D. N., Yanes, J. A., Pérez, A., Oudyk, K. M., Jarecka, D., Enge, A., Peraza, J. A., & Laird, A. R. (2022, January). *Neurostuff/nimare: 0.0.11* (Version 0.0.11). Zenodo. https://doi.org/10.5281/zenodo.5826281

Samara, A., Eilbott, J., Margulies, D. S., Xu, T., & Vanderwal, T. (2023). Cortical gradients during naturalistic processing are hierarchical and modality-specific. *NeuroImage*, *271*, 120023.

Shuman, D. I., Narang, S. K., Frossard, P., Ortega, A., & Vandergheynst, P. (2013). The emerging field of signal processing on graphs: Extending high-dimensional data analysis to networks and other irregular domains. *IEEE signal processing magazine*, *30*(3), 83–98.

Smith, R. E., Tournier, J.-D., Calamante, F., & Connelly, A. (2015). Sift2: Enabling dense quantitative assessment of brain white matter connectivity using streamlines tractography. *Neuroimage*, *119*, 338–351.

Spielman, D. A. (2007). Spectral graph theory and its applications. *48th Annual IEEE Symposium on Foundations of Computer Science (FOCS'07)*, 29–38.

Tewarie, P., Abeysuriya, R., Byrne, Á., O'Neill, G. C., Sotiropoulos, S. N., Brookes, M. J., & Coombes, S. (2019). How do spatially distinct frequency specific meg networks emerge from one underlying structural connectome? the role of the structural eigenmodes. *NeuroImage*, *186*, 211–220.

Tournier, J.-D., Smith, R., Raffelt, D., Tabbara, R., Dhollander, T., Pietsch, M., Christiaens, D., Jeurissen, B., Yeh, C.-H., & Connelly, A. (2019). Mrtrix3: A fast, flexible and open software framework for medical image processing and visualisation. *Neuroimage*, *202*, 116137.

Xu, H., Lorbert, A., Ramadge, P. J., Guntupalli, J. S., & Haxby, J. V. (2012). Regularized hyperalignment of multi-set fmri data. *2012 IEEE statistical signal processing workshop (SSP)*, 229–232.

Yamins, D. L., Hong, H., Cadieu, C. F., Solomon, E. A., Seibert, D., & DiCarlo, J. J. (2014). Performance-optimized hierarchical models predict neural responses in higher visual cortex. *Proceedings of the national academy of sciences*, *111*(23), 8619–8624.

Yang, Y., Zheng, Z., Liu, L., Zheng, H., Zhen, Y., Zheng, Y., Wang, X., & Tang, S. (2023). Enhanced brain structure-function tethering in transmodal cortex revealed by high-frequency eigenmodes. *Nature Communications*, *14*(1), 6744.

Yarkoni, T., Poldrack, R. A., Nichols, T. E., Van Essen, D. C., & Wager, T. D. (2011). Large-scale automated synthesis of human functional neuroimaging data. *Nature methods*, *8*(8), 665–670.

Yeo, B. T., Krienen, F. M., Sepulcre, J., Sabuncu, M. R., Lashkari, D., Hollinshead, M., Roffman, J. L., Smoller, J. W., Zöllei, L., Polimeni, J. R., et al. (2011). The organization of the human cerebral cortex estimated by intrinsic functional connectivity. *Journal of neurophysiology*.

Zhou, D., Zhang, G., Dang, J., Unoki, M., & Liu, X. (2022). Detection of brain network communities during natural speech comprehension from functionally aligned eeg sources. *Frontiers in Computational Neuroscience*, *16*, 919215.

Supplementary material

9 Structure-function relationship is not modulated by the salient events in the movie

Correlation of activity across subjects was quantified using Correlated Component Analysis (CorrCA; see Dmochowski et al., 2012 and Parra et al., 2018 for more details). In brief, CorrCA decomposes the data into components that maximize correlation across subjects. The correlated components were computed for cortical signals, and the Intersubject correlation (ISC) time series are presented in supplementary Fig 6ab, left. The strongest and weakest periods were then defined based on the ISC scores (dashed

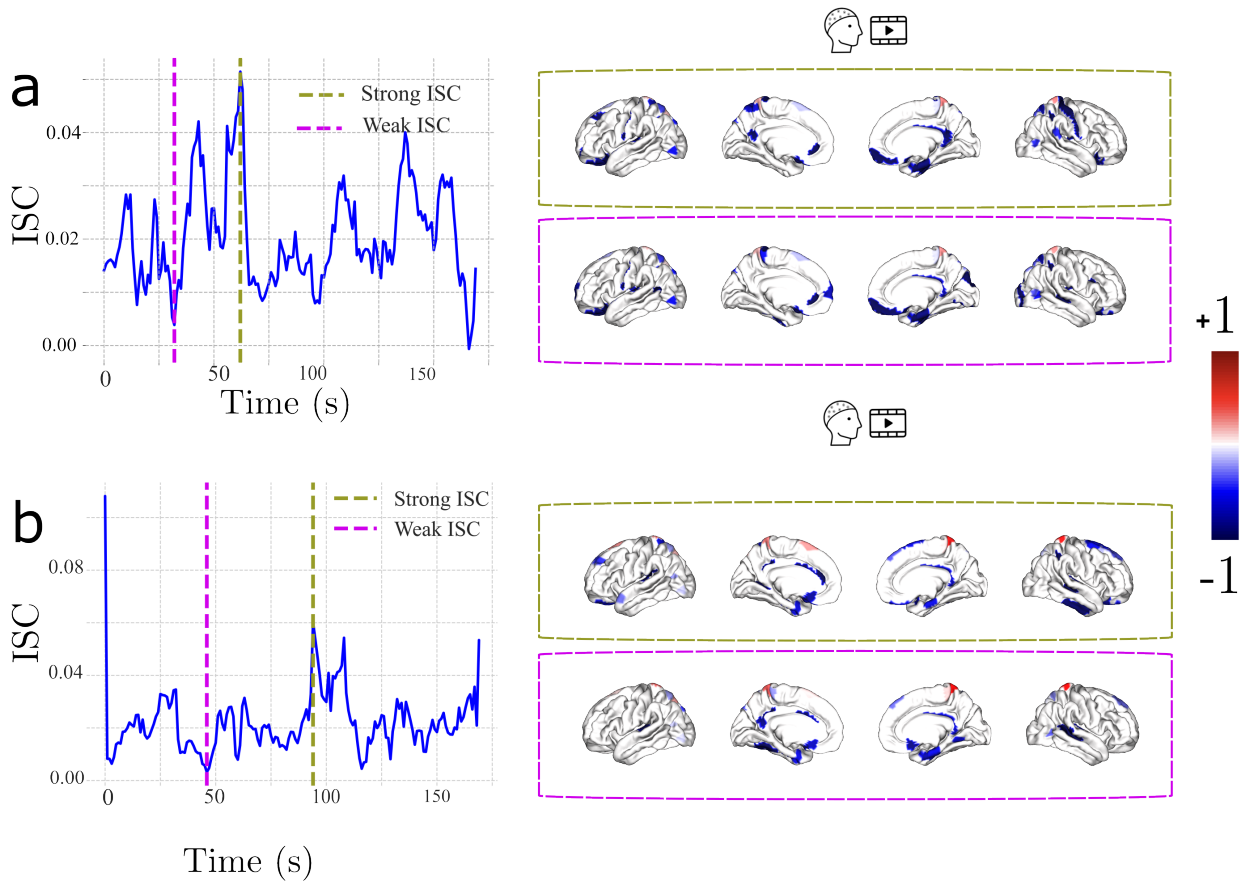

Figure 6: Structure-Function relationship during moments of strongest and weakest correlation in the cortical activity among subjects while watching Video 1. The correlation in the activity is estimated using CorrCA, and the first component capturing the correlation is presented in the left of both panels. Strong and Weak ISC periods are highlighted with the dashed line on the correlation time-series. On the right are the corresponding group-level SDI maps during these periods. Panel a and b present the results for wideband and theta band respectively.

line in Fig 6ab, left). The structure-function relationships of video-watching EEG were investigated for the aforementioned periods. Group-level SDI maps are presented for wideband (Fig 6a, right) and for the theta band (Fig 6c, right). We performed a statistical comparison between SDIs during moments of strongest and weakest correlation. The results indicated that there is no statistical difference between these moments. In sum, this analysis revealed that the SDI patterns are not modulated by the levels of correlation present in the cortical signal.